PHYSICAL REVIEW B VOLUME 7, NUMBER 2 15 JANUARY 1973

Recombination Processes Responsible for the Room-Temperature Near-Band-Gap Radiation from GaP

R. Z. Bachrach and O. G. Lorimor
Bell Laboratories, Murray Hill, New Jersey 07974
(Received 7 July 1972)

A detailed study has been made of the near-band-gap (green) radiative-recombination processes in GaP at room temperature for carrier concentrations small compared to the band density of states. This study has shown that for crystals with nitrogen concentrations lower than 10^{17} cm^{-3}, free-exciton recombination is the dominant process independent of the doping type or level. At nitrogen concentrations greater than 10^{18} cm^{-3}, nitrogen-related processes dominate the recombination. The recombination is primarily through a bound-exciton mode; however, it is shown that approximately 30% of the recombination proceeds through a free-exciton mode. No evidence of a free-to-bound process involving the nitrogen electron trap has been found with an upper bound on its strength of 10%. Free-to-bound recombination involving P-site neutral donors is found to be important in the temperature range 80–150 °K, but is unimportant at 300 °K. The spectra presented are corrected for the system response and obtained in a manner that eliminates bulk-absorption distortion. The spectra in this work represent the true internal-emission energy distribution.

I. INTRODUCTION

The near-band-gap (green) radiative-recombination processes in GaP have been studied as a function of impurity type for carrier concentrations small compared to the band densities of states at temperatures from 100 to 300 °K. A reinvestigation of this subject has been made to provide a more complete understanding of the radiative-recombination processes at room temperature in order to establish the basis for a kinetic model of green emission. The luminescent spectra were obtained so that they accurately approximate the internal-emission spectra and the spectra therefore establish the basis for measuring and calculating optical loss in GaP green diodes due to bulk absorption.

The primary interests of our investigation have been the room-temperature (~300 °K) spectra and radiative-recombination processes. Investigations of the spectra as a function of temperature, doping type, and concentration provide data for understanding the radiative processes and are presented to support the interpretations. Transient measurements are not presented in any detail here. As shown in a separate paper,[1] the transient response of the green luminescence over most of this temperature range is determined by other, deeper states, and the near-band-edge emission acts only as a probe. The primary character of the recombination processes discussed here is that they are strongly thermalized such that in the temperature range 100–300 °K, the whole spectrum, even though representing several processes, decays with the same time constant under transient excitation.

Most of the previous work on the subject[2–16] of the room-temperature near-band-edge recombination has utilized either diodes or cathodoluminescence. Reference 14 presents a recent summary of the previous work. We have found previous diode results on recombination processes in GaP to be ambiguous because comparably efficient recombination can occur from both the n- and p-doped side of the junction[17] and large self-absorption effects can distort the spectral line shapes. Self-absorption corrections have not been made in the previous work. All the processes discussed here have been proposed and discussed at some point in the literature; however, many of the results in the literature conflict in the identification of the important processes.

The work described here shows that the following near-band-gap processes are present at room temperature: (I) phonon- and impurity-assisted free-exciton recombination; (II) free-minority-to-bound-majority carrier recombination (or converse); and (III) bound-exciton recombination.

The most efficient near-band-edge room-temperature luminescence in GaP is aided by the addition of substitutional nitrogen which creates an electron trap.[18,19] We show that recombination induced by the nitrogen proceeds by both a bound-exciton[8,10] and a free-exciton mode.

In order to keep the discussion of the radiative processes succinct, combinations of impurities are selected to typify the results. At room temperature with substitutional nitrogen concentrations less than 10^{17} cm^{-3}, process I is found to dominate[1] independent of the majority-carrier dopant with net carrier concentrations investigated ranging from 5×10^{15} to 2×10^{18} cm^{-3}. The dopants investigated include S, Te, Si, Zn, Mg, and C, and thus span an impurity ionization range from 48 to 104 meV.[20] Process II provides only a weak low-energy shoulder at room temperature. Process-I spectra are defined with respect to Si-doped crystals since pro-

cess II is very weak. (This is generally true of Ga-site donors.) The presence of process II is demonstrated with S-doped crystals. Because S is one of the deeper donors, process II is reasonably separated from process I at lower temperatures. Process III is demonstrated with (S, N)- and (Zn, N)-doped crystals. Process III dominates in both n- and p-type crystals with nitrogen concentrations greater than 10^{18} cm^{-3}. Process I is important in such crystals and this is shown explicitly.

After a discussion of the experimental techniques, the spectral results are presented in Sec. III in subsections distinguished by the nitrogen concentration. These results are followed in Sec. IV by an analysis.

II. EXPERIMENTAL TECHNIQUE

A. Crystals

The samples studied were epitaxial crystals grown on liquid-encapsulated pulled-crystal GaP substrates.[21] The background net donor concentration $|N_D - N_A|$ in these crystals ranged from 1.0×10^{16} to 1×10^{17} cm^{-3} and is attributed primarily to Si. The sulphur and nitrogen (N) background is typically found from absorption measurements[22] to be $\lesssim 5 \times 10^{15}$ cm^{-3}. The minority-carrier lifetimes in these samples ranged from 70 to 200 nsec.[1] The initial crystal thicknesses were typically 30–50 μ.

The nitrogen concentrations [N] reported here from absorption measurements are based on the calibration scale originated by Cuthbert and Thomas.[23] Their scale had a quoted absolute accuracy of within a factor of 2–3. Recent measurements by Lightowlers[24] have indicated that this scale gives absolute nitrogen concentrations high by a factor of 5. In quoting the nitrogen concentrations here we have continued using the Cuthbert–Thomas scale. On this scale, the maximum nitrogen incorporated in liquid-phase epitaxial (LPE) growth is around 1.6×10^{19} cm^{-3}. Recent measurements indicate that vapor-phase epitaxial (VPE) growth incorporates considerably more nitrogen by a factor of 4–10.[25]

The length and width of the prepared sample specimens are large compared to the thickness. The samples are fabricated by polishing the growth face and then evaporating and alloying a (Be, Au) layer. The (Be, Au)-GaP interface reflectance was measured to be approximately 10%, so that the layer provides a highly absorptive, relatively energy-independent absorption which eliminates multiple-pass reflections. The layer is attached to a glass cover slide and the substrate lapped away to a typical working sample thickness between 15 and 25 μ. Samples as thin as 6 μ were investigated.

B. Apparatus

The spectra were obtained with a Spex 1401 double monochromator and an RCA C31000E photomultiplier used in a photon-counting mode. The detection apparatus has been described previously.[26] The raw spectra were normalized for the system response using computer analysis with a system response function measured directly using an Eppley standard lamp. Separate experiments have indicated that the normalization procedure is accurate to a few percent. The areas under the spectra were obtained by Simpson's-rule numerical integration of the experimental curves.

The variable temperature measurements were made with a Janis Super Vari-Temp He-gas-flow cryostat. The sample temperature was monitored above 100 °K with a copper-constantan thermocouple placed on the sample mounting block.

The samples were excited using the 4880-A argon-ion-laser line. The room-temperature absorption length of this line is 10.3 μ without nitrogen and 7.6 μ at 10^{19} cm^{-3} nitrogen. The laser beam was pulsed with a 10% duty cycle to eliminate heating and to take advantage of the greater luminescent efficiency at the higher excitation densities.[1] The spectra presented are independent of excitation density.

C. Measurement of Undistorted Spectra

Luminescent spectra that overlap regions of energy-dependent absorption become distorted so that the spectrum measured external to the crystal can be considerably different from the internal-emission spectrum. In indirect band-gap crystals such as GaP, the single-pass loss is not large and most of the spectral distortion arises from the multiple-path nature of photon escape.[27] For example, with 10^{19}-cm^{-3} nitrogen, the absorption at 300 °K is 400 cm^{-1} at 2.32 eV or 0.06 eV above the band gap.[8] At a nitrogen level of 10^{18} cm^{-3}, the major absorption over much of the spectrum results from the intrinsic absorption. By creating a strongly absorbing back surface on the crystals with the (Be, Au)-GaP alloy, the multiple-pass components are eliminated. Only light within approximately 17° of normal incidence escapes because the index mismatch between GaP and air prevents escape for larger angles of incidence due to internal reflection. The angular dependence of the escaping light can therefore be reasonably neglected, and the external spectrum $I_{ext}(E)$ is related to the internal spectrum by

$$I_{ext}(E) = I_{int}(E)\,(1-R) \int_0^d n(x)\, e^{-\alpha(E)x}\, dx \,, \qquad (1)$$

where R is the interface reflectivity and d the crystal thickness. If $\alpha(E)x$ is small over the range

of interest, then $e^{-\alpha(E)x} \approx 1$ and the external spectrum equals the internal spectrum independent of the generation profile $n(x)$. For a 25-μ-thick layer with the highly absorbing back surface, the spectra obtained are good for absorptions less than 400 cm^{-1}.

Undistorted spectra therefore have been obtained in this work by creating a first-pass geometry. Figure 1(a) gives an example. The solid curve shows the 300 °K internal spectrum obtained in this work by the above procedure for 10^{19}-cm^{-3} nitrogen. The dashed curve is an external spectrum typical of those seen from GaP diodes doped with 10^{19}-cm^{-3} nitrogen. Figure 1(b) shows a comparison of the internal spectrum with the intrinsic and nitrogen-doped absorption spectra.[8] The nitrogen absorption scales linearly with the nitrogen concentration. Similar differences can be demonstrated with the spectra from non-nitrogen-doped crystals. For optical coupling in the multiple-bounce mode, the crystals are relatively opaque at absorptions of 50 cm^{-1}.[27]

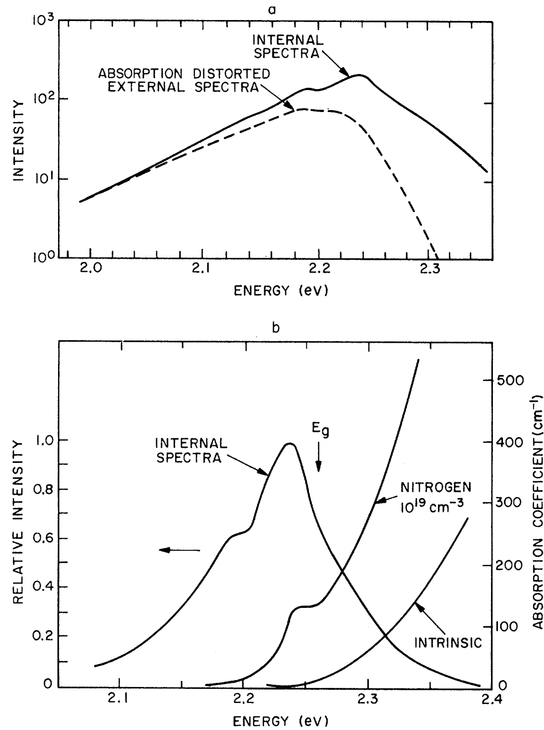

FIG. 1. (a) An example of the internal luminescent spectra obtained in this work compared with a bulk-absorption-distorted electroluminescent-diode external spectrum. The crystals are doped to 10^{19}-cm^{-3} nitrogen. The spectra are plotted on a logarithmic intensity scale versus energy. (b) A comparison of the internal luminescent spectrum for 10^{19}-cm^{-3} nitrogen with the intrinsic and nitrogen-related absorption spectra.

III. SPECTRAL RESULTS

The spectral results are organized into three sections distinguished by nitrogen concentration. This has provided a convenient breakdown of a multiparameter study. Fortunately, there is sufficient simplicity in these results to allow generalization from a few representative examples.

A. Nitrogen Concentration less than 1×10^{17} cm^{-3}

The crystals discussed in this section have substitutional nitrogen concentrations less than 5×10^{15} cm^{-3}. They are representative for temperatures above 250 °K of crystals with $[N] < 1 \times 10^{17}$ cm^{-3}. Figures 2(a) and 2(b) show the normalized spectral results obtained with Si- and S-doped crystals plotted as relative intensity versus energy as a function of temperature. The arrows indicate the free-exciton band gap at each temperature. The differences in the line shape at 300 °K as a function of the majority-carrier dopants investigated can be attributed to weak features on the low-energy tail. This can be seen in the Si and S spectra in Fig. 3 with the spectra plotted on a logarithmic scale. The primary recombination at 300 °K is shown in Sec. IV B to be due to phonon-assisted free-exciton recombination. This process has been found to be independent of the majority-carrier dopants investigated, C, Mg, Zn, Te, Si, and S, thus spanning an ionization-energy range 48–104 meV.[20] The low-energy tail variations are shown in Sec. IV C to result from a free-to-bound recombination whose details are dependent on the specific dopant involved.

As discussed in Sec. IV, the primary spectral components in Fig. 2(a) are due to phonon-assisted free-exciton recombination. In Fig. 2(b), one sees at low temperatures additional structure absent from Fig. 2(a). This includes a free-to-bound transition involving the neutral sulphur donor near 2.24 eV and a bound exciton on the sulphur donor near 2.30 eV.

At temperatures below 200 °K, resolvable structure appears in all the spectra and these various lines can be related to the processes taking place. This is done in Sec. IV. Below about 150 °K, strong donor-acceptor pair bands appear.[28] Pair-spectra transitions have been amply treated elsewhere and are not shown in detail here.[29,30] Pair recombination has not been found to be an important part of the near-band-edge spectra at 300 °K.

B. Transition Region: $10^{17} \leq [N] \leq 10^{18}$ cm^{-3}

By the transition region we mean those nitrogen concentrations for which the importance of the various processes is rapidly changing. An exhaustive study of this region has not been made. The characteristic of this region is, however, that one is going over from a regime where the nitrogen

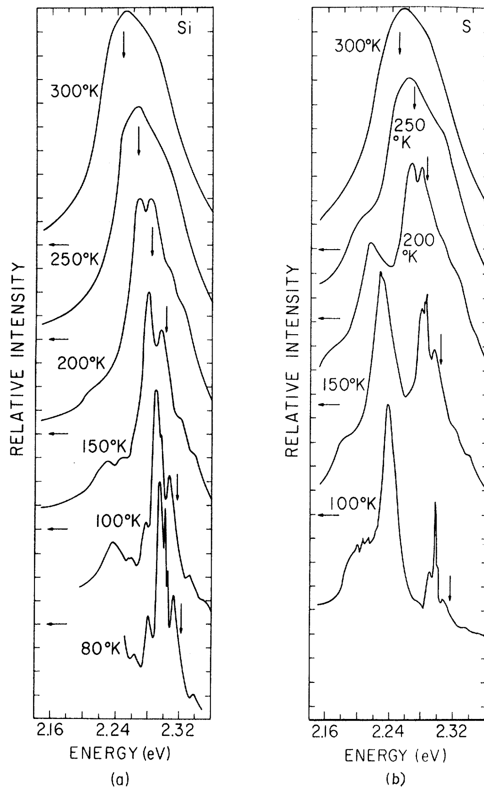

FIG. 2. Relative intensity spectra (normalized for system response) versus energy as a function of temperature for (a) Si-doped crystal ($N_D = N_A = 2\times10^{17}$ cm^{-3}) and (b) a S-doped crystal ($N_D - N_A = 4\times10^{17}$ cm^{-3}). An important attribute of all the spectra in this paper is that they are corrected for the system response and obtained so that they are undistorted by bulk self-absorption.

is not important to one in which the spectrum is dominated by the nitrogen and becomes approximately independent of the nitrogen concentration.

Figure 3 shows the comparative 300 °K spectra as a function of nitrogen concentration. One sees that at $[N]\approx 1\times10^{17}$ cm^{-3}, the bound-exciton transition on the nitrogen is barely resolved from the free-exciton recombination. Above 10^{18}-cm^{-3} nitrogen, the spectrum becomes approximately independent of the nitrogen concentration. One finds, however, small additional changes on the high-energy side between 10^{18}–10^{19}-cm^{-3} nitrogen.

The detailed temperature dependence of the spectra in the transition region is complicated and not very fruitful to show. One typically sees the bound-exciton component increasingly dominating the spectra as the temperature is lowered and the thermalization time of the nitrogen bound exciton becomes longer. With $[N]=10^{17}$ cm^{-3}, clearly resolved bound-exciton components can be seen at 150 °K.

C. Nitrogen Concentration greater than 10^{18} cm^{-3}

Above 10^{18}-cm^{-3}-nitrogen level, the same internal spectrum is obtained at 300 °K independent of the majority-carrier-dopant type or concentration ($5\times10^{15}\le |N_D - N_A| \le 2\times10^{18}$ cm^{-3}). The temperature dependence of the nitrogen spectra is complicated by the presence of the N-N-pair transitions.[19] Their contribution to the lower-temperature spectra is a function of both the nitrogen concentration and the position of the Fermi level. This is discussed further in Sec. IV D.

Figure 4 shows the spectral dependence of a (S, N)-doped crystal with $N=2\times10^{18}$ cm^{-3} and $N_D - N_A = 2\times10^{17}$ cm^{-3}. Even at 100 °K the N-N-pair bound-exciton lines have not appeared, while in similar p-type samples they are quite important by 200 °K. These data will be discussed in Sec. IV D. The structure resolved in Fig. 4 can be readily assigned by comparison with 4 °K spectra[19] and shown to correspond with the various nitrogen-bound-exciton features.

The N-N-pair lines have not been found to be of any consequence at room temperature in the samples investigated in this work. These have a maximum nitrogen concentration of 1.6×10^{19} cm^{-3} (3.2×10^{18} cm^{-3} on the Lightowlers's scale). The importance of the N-N-pair bound-exciton transitions at 300 °K in VPE samples with higher nitrogen concentrations could be considerably enhanced.

IV. ANALYSIS OF RESULTS

A. Recombination Processes

The recombination processes occurring can be distinguished on the basis of the temperature dependence of the peak energy relative to the band gap, changes in the line shape with temperature, and impurity and carrier concentration dependences. The energy discrimination is accomplished by the

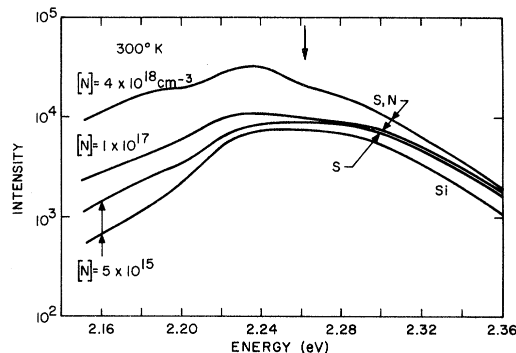

FIG. 3. Spectral changes as a function of nitrogen concentration for sulphur-doped layers. A Si-doped crystal spectrum is also shown to emphasize the differences between the spectra on the low-energy tail.

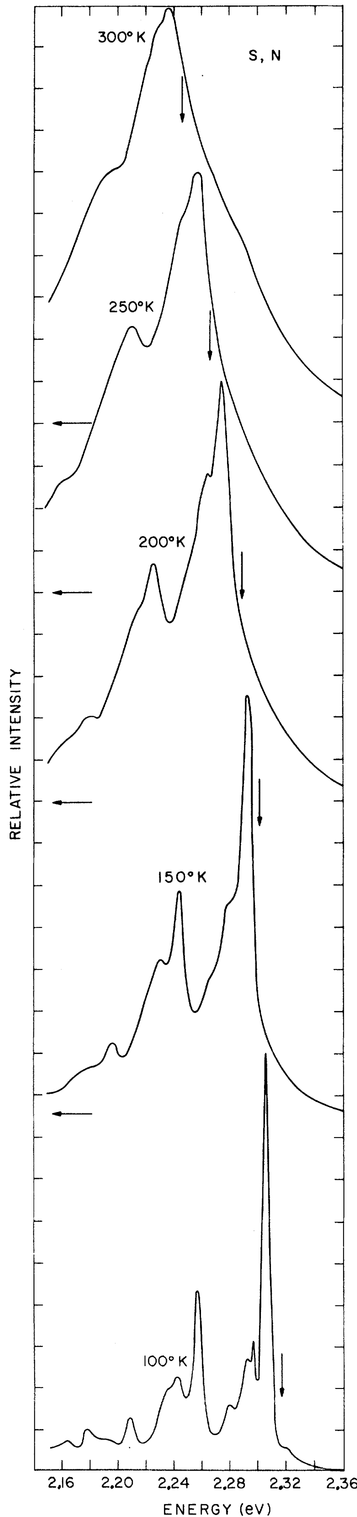

FIG. 4. Relative intensity spectra (normalized for system response) versus energy for a S-doped crystal ($N_D - N_A = 2\times 10^{17}$ cm^{-3}) with a nitrogen concentration of 2×10^{18} cm^{-3}. A weak feature due to the sulphur bound exciton can be seen in the 100 °K curve.

energy balances listed below for the various processes.

1. Free-exciton (phonons and impurity assisted) $\kappa = 1$ state:

$$E = E_g - E_{fx} + \Delta KE_{fx} \pm n\hbar\omega,$$

$n \geq 1$ phonon assisted, $n \geq 0$ impurity assisted. (2)

1′. Free-electron hole ($\kappa = 2$–∞ exciton state):

$$E = E_g + \Delta KE_e + \Delta KE_h \pm n\hbar\omega, \quad n \geq 1 . \tag{3}$$

2. Bound exciton:

$$E = E_g - E_{fx} - E_{bx} \pm n\hbar\omega, \quad n \geq 0 . \tag{4}$$

3. Free to bound (electron or hole bound):

$$E = E_g - E_{D,A,I} + \Delta KE \pm n\hbar\omega, \quad n \geq 0 . \tag{5}$$

κ is the orbital quantum number, E_g is the one-electron band gap, E_{fx} is the free-exciton binding energy, ΔKE results from the peak shift due to a free carrier or free exciton being involved, E_D, E_A, and E_I are the binding energies for donors, acceptors, or isoelectronic traps, E_{bx} is the bound-exciton binding energy, n is the number of phonons involved, and $\hbar\omega$ is a phonon energy. The important phonons for GaP are the transverse optical (TO), longitudinal optical (LO), and transverse acoustic (TA). The indices LO^Γ or LO^X, etc., refer to the phonon energies at particular symmetry points in the Brillouin zone. Several comments should be made concerning these relations.

(i) Applying the energy balances in the cases of the process with one or both carriers free requires a knowledge of the intensity as a function of particle kinetic energy in order to relate peak positions to other measurable parameters.[31] The intensity of the emitted light is determined by

$$I(E) = N(E)/\tau(E) ,$$

where $N(E)$ is determined by the thermalization of the available carriers over the density of states and $\tau(E)$ is the reciprocal of the recombination rate and, depending on the process, may or may not be energy dependent. This line shape determines the peak of the transition. Generally the thresholds are not as clearly resolved as they are in absorption measurements.

(ii) Because of the important phonon participation, the zero of the system can be determined when it is possible to resolve either a zero-phonon line or both the Stokes and anti-Stokes components. Thus the quantities $(E_g - E_{fx} - E_{bx})$ can be determined with precision. Such measurements have been carried out in absorption to determine the free-exciton band gap $E_g - E_{fx}$.[32,16] Other measurements referenced to the nitrogen-bound-exciton luminescence have also been carried out by both absorption[33] and differential absorption.[34] The agreement of the various measurements is quite

good. Since the relevant energies for analysis of the spectra are relative to the band gap, previously presented spectra are replotted below with an energy scale relative to the free-exciton–band-gap data obtained from Ref. 32. This type of energy scale clearly shows variations that are distorted in the raw data because of the systematic shift in energy of the spectral features with temperature owing to changes in the band gap.

(iii) Pertinent to the analysis of the various spectral results are the various physical parameters of GaP. Table I lists some of the currently accepted binding energies and phonon energies for GaP. Many of the values listed were determined at low temperatures (< 10 °K) so that some change is likely to occur in these values at room temperature. Of the parameters that are varying, $E_g - E_{fx}$, the free-exciton energy gap, is perhaps most accurately known. The free-exciton energy gap should represent the band-gap change accurately because the exciton binding energy does not change more than a few percent from 4 to 300 °K. The binding energy of a Wannier exciton is related to various effective mass parameters by[35]

$$E_{fx} = \mathcal{R}\mu^*/\epsilon^2 ,$$

where $\mathcal{R}$ is the hydrogenic Rydberg, μ^* is the reduced mass, and ϵ is approximately the static dielectric constant. This changes from 11.1 at 300 °K to 10.85 at 4 °K.[36,37] Changes in the reduced mass would be expected to be small. One finds from the difference between the nitrogen-bound-exciton position and the free-exciton band gap that both the binding energies are relatively temperature insensitive.[32,33] A similar conclusion has been reached with respect to the (Zn, O) center.[38]

TABLE I. Binding energies and phonon energies for GaP.

Binding energies (meV)			Phonon energies (meV)
Free exciton	Impurity	10 ± 1[a]	LO^{Γ} 50.3 ± 0.5[a–d]
Bound exciton	N	11 ± 1[b]	TO^{Γ} 46.5 ± 0.5
	Bi	97 ± 1[b]	LA^{X} 31.3 ± 0.6
	S	18.9 ± 1[c]	TA^{X} 12.8 ± 0.5
	Te	18.9 ± 1[c]	LO^{X} 44.4 ± 0.5
	Zn	6.7 ± 1[d]	TO^{X} 46.5 ± 0.5
Donor or acceptor energy	S	104.0[d]	
	Te	89.5[d]	
	Si	82.0[d]	
	Zn	63.0[d]	
	C	45.5[d]	

[a]Reference 32.
[b]Reference 23.
[c]P. J. Dean, Phys. Rev. 157, 665 (1967).
[d]Reference 47.

B. Process I: Phonon-Assisted Free-Exciton Recombination

The Si spectra shown in Fig. 2(a) are replotted in Fig. 5 with the energy relative to the band gap. The relationship and variation of the spectral features as a function of temperature are seen quite clearly in this type of presentation. The Si spectrum in the range 100–300 °K results predominantly from phonon-assisted free-exciton recombination, as is shown below. This process is also clearly discerned in the sulphur spectra in Fig. 6.

The components in the free-exciton spectra arise from the annihilation of a mobile exciton with the emission or absorption of a phonon. By comparing the spectra with the absorption curves of Dean and Thomas,[32] the spectral features can be associated with the TA, LA, and TO phonons.[12,15,16] With reference to the 100 °K curve in Fig. 4, these include the – TO peak near – 40 meV, the – LA peak near – 25 meV, the – TA peak near – 10 meV, and the TA peak near 19 meV. The LO mode is not present because of the selection rules.[32] Figure 7 demonstrates the processes schematically utilizing the phonon energies measured by Dean and Thomas. One has a series of thresholds at the one-phonon and multiple-phonon energies. Processes that involve the absorption of a phonon have a vanishing transition rate as $T \to 0$. At temperatures such that the thermal energies are low compared to the available momentum-conserving phonon energies, the spectra consist predominantly of phonon-emission-assisted processes. Because of momentum conservation, there is no first-order process. A zero-phonon free-exciton recombination line has not been seen in this work. However, a zero-phonon line has been observed at very low temperatures in GaP crystals containing small amounts of As.[16] Similar breakdowns in the selection rules have been observed in absorption in mixed crystals.[39,40]

The phonon-assisted peaks have been investigated via the temperature dependence of the peak position and the spectral intensity. The emission line shape above threshold is determined in the simplest exciton model by the thermalization of the excitons over the available density of states, since the transition time $\tau(E)$ should be independent of energy. The thermal distribution is maintained primarily by scattering with low-energy small-wave-vector acoustic phonons. This scattering process, depicted in the inset in Fig. 7, redistributes the transition oscillator strength, but does not change it. The line shape is then given by

$$F(E, T) = \frac{2}{\sqrt{\pi}} \left(\frac{1}{kT}\right)^{3/2} \sqrt{E}\, e^{-E/kT} \qquad (6)$$

and has a temperature-independent area. From this relationship, one can easily show that the peak height decreases inversely with temperature and correspondingly the half-width increases linearly with temperature. The actual half-width is given

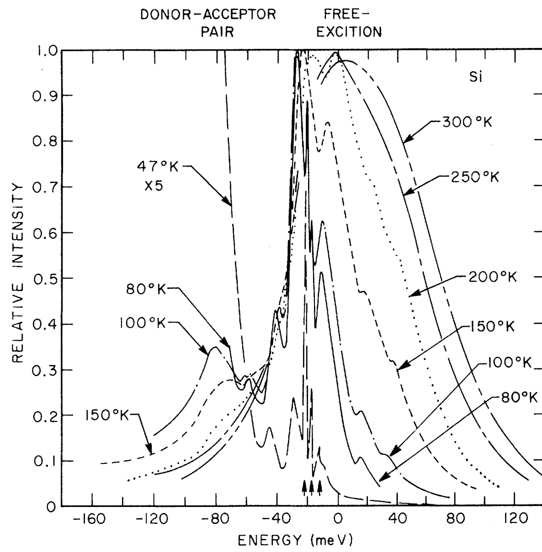

FIG. 5. Relative intensity spectra (normalized for the system response) versus energy relative to the free-exciton band gap. The crystal is the same one shown in Fig. 2(a). This manner of presentation shows clearly that the spectral process changes with temperature. The spectra are arbitrarily normalized to a peak height of unity. The absolute peak-height relationships as a function of temperature have not been measured. The three arrows mark the Si-bound-exciton triplet.

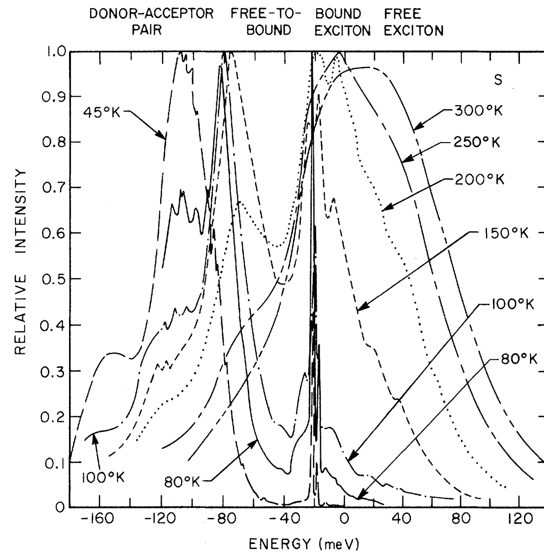

FIG. 6. Relative intensity spectra (normalized for the system response) versus energy relative to the free-exciton band gap. The crystal is the same one shown in Fig. 2(b). The figure is complicated by the presence of four recombination processes that have different temperature dependences. The region near −20 meV is dominated by the S bound exciton which at lower temperatures overlies the weaker free-exciton recombination. The low-temperature free-exciton components are seen more clearly in Figs. 2 and 5. This figure is meant to emphasize the relative temperature dependences of the four processes.

approximately by

$$\Gamma \simeq 1.8kT . \tag{7}$$

With this line shape, the luminescence from a free-exciton process should peak at

$$\Delta E_{KE} \simeq kT/2 \tag{8}$$

above threshold and therefore shift systematically with temperature relative to the band gap.[12]

Figure 8 shows the peak position relative to the free-exciton band gap of the phonon-emission-assisted features versus temperature. The LA feature is most clearly resolved and the data for it fit a straight line quite well. The slope of $(0.58 \pm 0.1)k$ is in agreement with the expectation of the simple exciton model. The extrapolation of the line to $T=0$ from Eq. (2) gives an LA-phonon energy of 32 ± 1 meV, in good agreement with the currently accepted value listed in Table I of 31.3 ± 0.6 meV. The TO and TA modes also shown in Fig. 8 are weaker transitions and the line shapes are more easily disturbed by overlapping processes. For example, the TO line is not resolvable above 120 °K. Both the LA and TA peak positions deviate from the expected relation above about 160 °K. This is discussed further below and is related to the broadening and overlap of the various features. The data for these other features are consistent

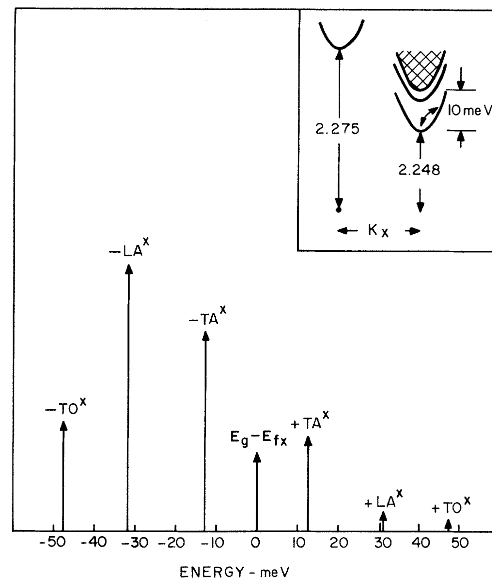

FIG. 7. Schematic representation of the primary phonon contituents in the phonon-assisted free-exciton recombination. The inset depicts the excitonic band structure and thermalization within the exciton band.

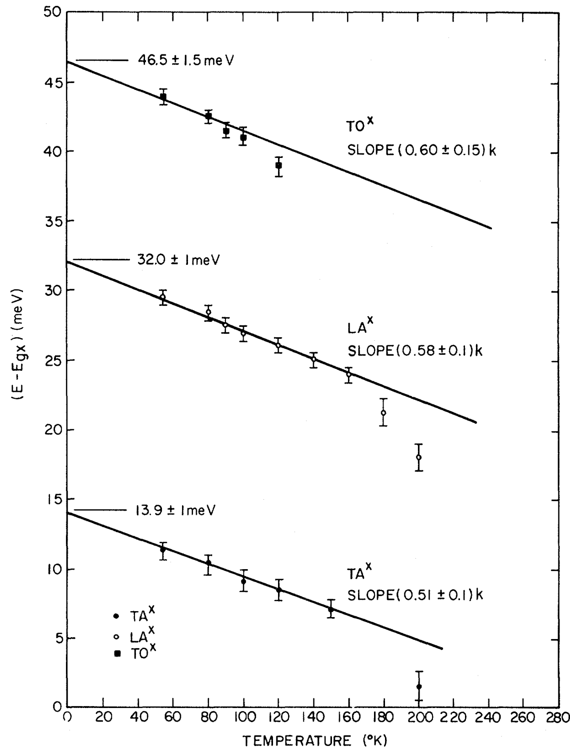

FIG. 8. Peak position relative to the free-exciton band gap versus temperature for the TA^X, LA^X, TO^X modes in the free-exciton spectra. The extrapolations to zero temperature indicate phonon energies in agreement with the currently accepted values. The line slope is within a range expected for a model accounting for exciton thermalization.

with their interpretation and they yield similar slopes.

Examination of Fig. 5 or 6 shows the manner in which the phonon absorption components, i.e., the high-energy side of the spectra, increase with temperature. These spectral changes can be understood on the basis of changes in phonon population with temperature. The phonon occupation numbers for the TA and LA phonons

$$n(T) = \frac{1}{e^{\hbar\omega/kT} - 1} \tag{9}$$

are shown in Fig. 9 along with the ratio n_{TA+1}/n_{LA+1} and the energy equivalent of the temperature. The transition rate for the free-exciton recombination has the transition matrix element .odulated by a phonon occupation number. The Stokes-to-anti-Stokes intensity ratio is

$$R = n/(n+1) = e^{-\hbar\omega/kT}, \tag{10}$$

where n is the phonon occupation number and $\hbar\omega$ is the phonon energy. Figure 10 plots the Stokes–anti-Stokes intensity ratio of the TA and LA emis-

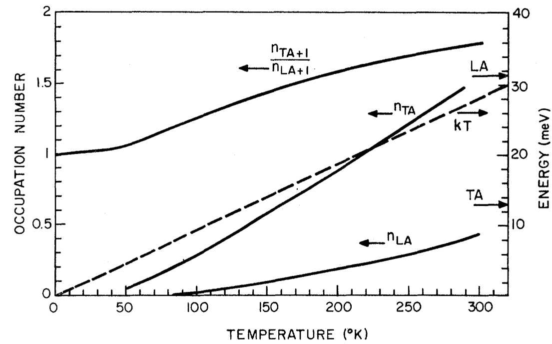

FIG. 9. Solid lines show the phonon occupation numbers versus temperature and the $(n+1)$ ratios for the TA^X and LA^X modes. The dashed line shows the energy equivalent of temperature. The spectra shown in Figs. 4 and 11 become indistinct around 200 °K where the TA^X-phonon occupation number approaches unity.

sion peaks versus $1/T$. Both of these show an activation energy consistent with the process assignment to TA and LA phonons. The temperature dependence of the spectra can therefore be understood simply on the basis of the TA- and LA-phonon populations. Following the ratio above about 200 °K is difficult because of the overlap of the various processes and the increasing importance of higher-

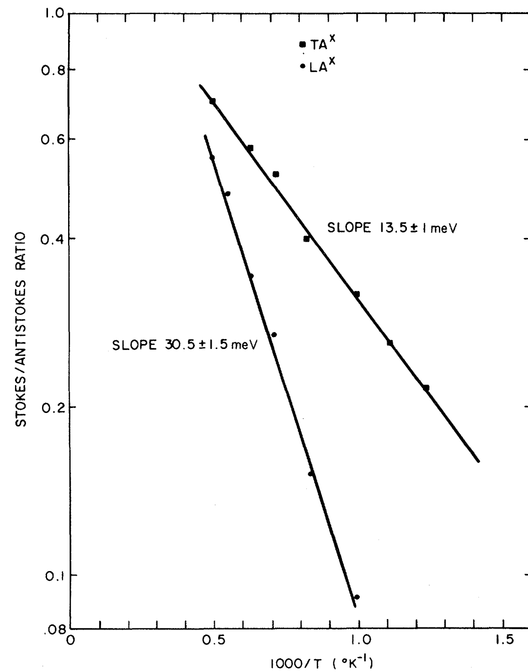

FIG. 10. Ratio of the phonon-emission to phonon-absorption peak heights is plotted versus inverse temperature for the TA^X and LA^X modes. The slopes yield a phonon energy in agreement with the currently accepted values.

order (i.e., multiple-phonon) processes. The increasing phonon population increases the absolute area and therefore the peak height decreases more slowly as the temperature increases than Eq. (6) suggests. This area increase is related to an increase in the over-all transition strength. It has not been possible to measure the absolute relation of the peak heights as a function of temperature for the following reasons: (a) The crystals are very thin and much of the input power is not absorbed in the crystal and the absorbed fraction is a strong function of temperature. (b) The strength of the minority-carrier shunt path[1] (nonradiative minority-carrier recombination paths) and the majority-carrier concentrations are strong functions of temperature. The area change can be estimated, however, because the peak heights of the transitions can be determined at low temperatures where the lines are fairly well resolved and the occupation numbers are close to zero. For example, at 50 °K, $n+1$ for the TA mode is only 1.054. The temperature-independent strength ratio for the TO, LA, and TA modes has been found to be 1: 3.75: 1.5. The area $A(T)$, and therefore the transition strength, changes with temperature according to

$$A(T) = 0.154\,[2n_{\mathrm{TO}}(T)+1] + 0.615\,[2n_{\mathrm{LA}}(T)+1] + 0.231[2n_{\mathrm{TA}}(T)+1] . \quad (11)$$

As the n's go to zero, the normalized area goes to the temperature-independent value of unity. The coefficients in this relation are related to the exciton-phonon interaction matrix elements for the various modes. One finds from this that the free-exciton transition strength is enhanced at room temperature by a factor of 2.3 because of the increased phonon population.

The effective transition rate for the free-exciton recombination was determined from low-temperature absorption measurements by Dean *et al.*[8] The value of $B = 10^{-13}$ cm^3/sec is a function of temperature given by

$$B(T) = A(T) \times 10^{-13} \text{ cm}^3/\text{sec} .$$

At room temperature this implies for $p = 10^{17}$ cm^{-3} that the radiative time constant is approximately 40 μsec. This is about 20–40 times larger than a transition time one would estimate for the nitrogen bound exciton at 10^{19}-cm^{-3} nitrogen concentrations. The implication of this is that the phonon-assisted free-exciton mechanism is intrinsically less competitive than the nitrogen-bound-exciton recombination.

Although it has not been possible to measure the absolute area change, a check on the result can be obtained by comparing the room-temperature spectrum with that calculated using the measured strength ratios and the line shape. This has been done for a relative normalization and is shown in Fig. 11 as the solid curve. The line shape was derived by summing over the three emission and absorption modes multiplied by the temperature-independent strength ratios and the phonon occupation factors.

One sees that the comparison is quite good, even though no attempt has been made to include broadening of the threshold or the important multiphonon processes. This comparison provides the strongest support for the room-temperature-process assignment. This identification can be stated differently. One should note that $kT/2$ at room temperature is approximately 12.5 meV and that the spectra are centered by about this energy above the free-exciton band gap. If the primary process were free-electron–hole recombination, then the peak would be expected to occur considerably above the free-electron band gap, or approximately 35 meV above the free-exciton band gap. This is clearly resolved not to be the case.

The phonon-assisted free-exciton spectra in GaP were first identified by Wight.[12] The spectral line shapes were subsequently studied in detail in the temperature range below 70 °K by Mosby, Lightowlers, and Davies[16] and they found that emission com-

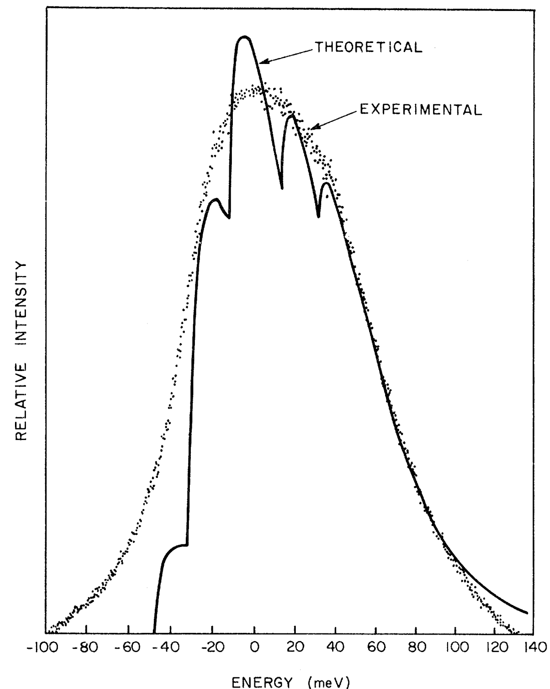

FIG. 11. Comparison of the measured spectral line shape for the free-exciton emission with that calculated by summing over the one-phonon modes in the recombination model. Broadening of the threshold and higher-order phonon processes were not included.

ponents fit Eq. (6) quite well. Our analysis of the phonon-assisted free-exciton spectra is in agreement with these works. This work has shown the high-temperature character of the recombination in these crystals more clearly than the previous work.[12,15,16] We return to a discussion of the free-exciton recombination in Sec. IV D.

C. Process II: Free to Bound

In the case of a free-to-bound process[6-8,31,41,42] $\tau(E)$, the recombination time can depend on energy through the thermal valocity of the carriers and the energy dependence of the capture cross section. The capture time of a free particle can be represented by[43]

$$\tau = 1/N_t \sigma(T) V_{\text{th}} , \tag{12}$$

where N_t is the trap density, $\sigma(T)$ the temperature-dependent capture cross section, and V_{th} is the mean thermal velocity. The emission intensity is then given by

$$I(E) = N(E) N_t \sigma(t) V_{\text{th}} \propto N_t \sqrt{E}\, e^{-E/kT} \sqrt{E}\, \sigma(E) \approx N_t \sigma(E) E e^{-E/kT} . \tag{13}$$

If the cross section were independent of energy, then the band would peak at $E \sim kT$ above threshold.

Figure 12 shows a plot of the peak position relative to the free-electron band gap for the peak in the sulphur spectrum [Figs. 2(b) and 6] associated with the free-to-bound process. Extrapolation to $T = 0$ yields a donor binding energy relative to the free-electron band gap of $E_D = 101.5 \pm 2$ meV, in reasonably good agreement with the currently accepted experimental value of 104 meV.[44] The result of Fig. 12 and the line shape indicate that this is a zero-phonon transition. The slope of the line of $1.4k$ suggests the capture cross section has an energy dependence close to $\sqrt{E}$.

The assignment of this band depends on the peak shift with temperature, as well as the temperature dependence of the intensity. The latter is shown in Fig. 6, which is complicated by four competing processes that are all changing in different ways as the temperature increases. With reference to the 45 °K curve in Fig. 6, the spectra consist primarily of a C-S pair band[45] peaking near − 110 meV and a bound-exciton recombination on a neutral sulphur donor. (The peak of the pair band is shifted to higher energy because of the high excitation density.[29]) Examination of Fig. 6 reveals the evolution of these processes. The 45 °K curve shows the D-A band and the bound-exciton band. Only as the unintentionally present C acceptors begin to thermalize does the new band appear. This is already quite pronounced at 80 °K. One can see the peak shift to higher energies as the temperature increases from 80 to 200 °K. Above 150 °K, the

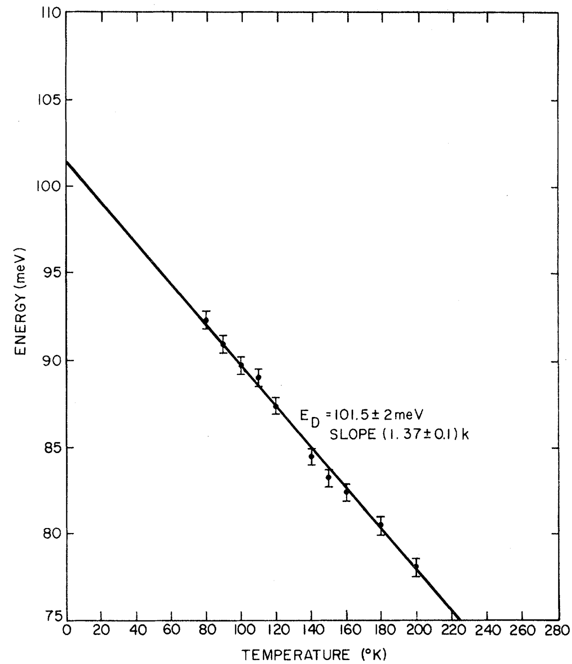

FIG. 12. Peak position relative to the free-electron band gap versus temperature for the sulphur free-minority-to-bound-majority carrier recombination. Extrapolation to zero temperature yields a donor-ionization energy (relative to the free-electron band gap) in agreement with the currently accepted value. The slope of the line indicates the neutral-donor hole-capture cross section has approximately a one-half-power dependence on carrier kinetic energy.

bound-to-free band begins to fall rapidly and the free-exciton band increases as the neutral sulphur donors thermalize appreciably.

Figure 13 shows qualitatively similar behavior for a Zn-doped sample, but there are important differences. The pair band is due to Zn-S pairs[46] and persists to much higher temperatures. The onset of the free-to-bound band also occurs at higher temperatures; for example, compare the 80 °K curves in Figs. 6 and 13. These differences result because the deeper Zn acceptor level thermalizes at higher temperatures. The weakness of electron scattering at a neutral acceptor in GaP[47] manifests itself in Fig. 13 by the apparent absence of both a bound exciton and a free-to-bound transition involving the neutral zinc acceptor. At low temperatures the residual S background dominates the spectra. Sulphur has been shown to have a large capture cross section for electrons.[48,49] The free-to-bound process in the Zn-doped samples involves a bound minority carrier and a free majority carrier. This is the converse of what is seen in the n-type sample.

The free-to-bound processes occur on neutral

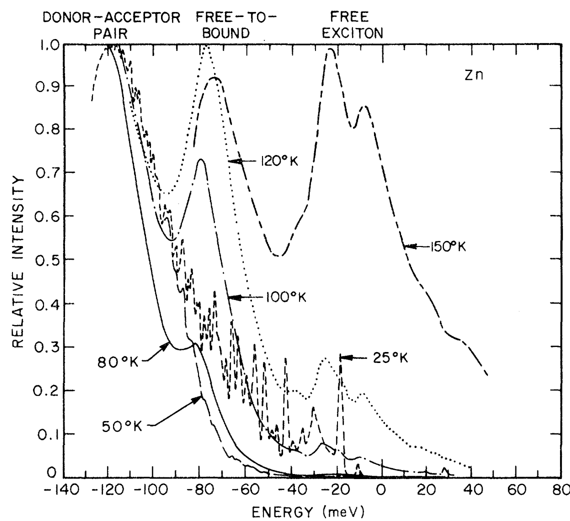

FIG. 13. Relative intensity spectra (normalized for the system response) versus energy relative to the free-exciton band gap for a Zn-doped crystal ($N_A - N_D = 2.5 \times 10^{17}$ cm^{-3}). The major impurity background is due to sulphur.

centers in the temperature range where the bound exciton has strongly thermalized, but the center is still predominantly occupied. The free-minority-to-bound-majority recombination (or converse) is not found to be a dominant process at room temperature for the majority-carrier concentrations ($|N_D - N_A| \lesssim 2\times10^{18}$ cm^{-3}) investigated. A remnant of this band can be seen in the low-energy tail of the spectra. For example, in Fig. 3 one can see a spectral difference in the spectra between 2.16 and 2.20 eV for Si and S which can be accounted for by process II. The temperature dependence of the spectra is particularly graphical and provides insight into the impurity electron kinetics.

Several of the earlier works on this subject using spectra from electroluminescent diodes concluded that process II was most responsible for the room-temperature luminescence in GaP when N was absent.[6,8] The errors in these works are most likely due to the large self-absorption distortion of the spectra. The result of the present work (that it is the excitonic processes, both free and bound, that are important at room temperature) seems to be generally applicable to GaP. Recent theoretical work had predicted that process II would be very important in both the N-doped and (Zn, O)-doped crystals.[50] This is not substantiated.

We conclude this subsection by discussing the differences between the Si- and S-doped spectra in Figs. 5 and 6. The major difference results from the weakness of the free-to-bound recombination on the neutral Si donor. This can be explained on the basis of the selection rules pertaining to a Ga-site donor in GaP,[51] the free-to-bound transition being forbidden by the recombination symmetry selection rules. The other differences arise from the effect of site symmetry on the bound exciton. One sees weakly in the 80 °K curves in Figs. 2(a) and 5, and also strongly in the 47 °K curve in Fig. 5, that additional structure appears within the free-exciton spectra. This weak triplet structure (marked by arrows) arises from a bound-exciton transition at neutral silicon donors.[52] The relative strength of the S-bound exciton can be seen from the ratio of the bound-exciton peaks to the free-exciton features. The sulphur-bound exciton remains a prominent feature to much higher temperatures. The region near – 20 meV in Fig. 6 is obscured by the overlapping bound-exciton peaks.

The donor-acceptor pair recombination in this sample results from both Si-Si and C-Si pairs.[45] The C-Si band quenches rapidly as the shallow C thermalizes, although the remnant is present to 150–200 °K. The Si-Si pair band can be followed to 300 °K.[22]

D. Process III: Bound Exciton

Figures 14 and 15 show spectra for nitrogen-doped samples with the energy measured relative to the free-exciton band gap. The sample shown in Fig. 14 is *n* type while that shown in Fig. 15 is *p* type. The principal features in these spectra arise from bound-exciton recombination. The

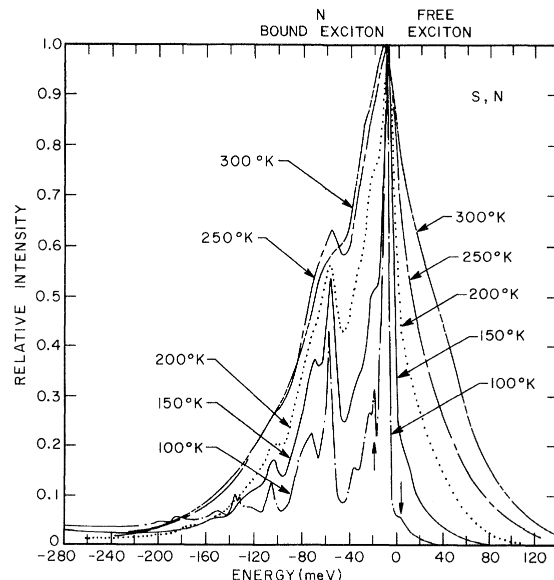

FIG. 14. Relative intensity spectra (normalized for the system response) versus energy relative to the free-exciton band gap. The crystal is the same one shown in Fig. 4. Note the *A* line evolves continuously versus temperature without changing position relative to the free-exciton band gap.

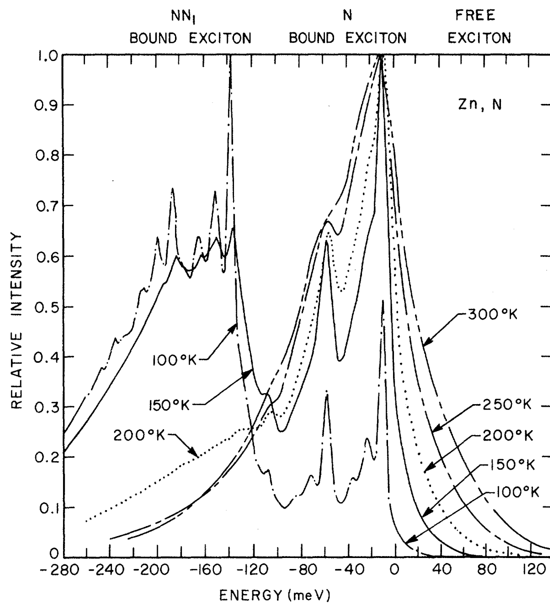

FIG. 15. Relative intensity spectra (normalized for the system response) versus energy relative to the free-exciton band gap for a Zn-doped crystal ($N_A - N_D = 7 \times 10^{17}$ cm^{-3}) with 1×10^{19}-cm^{-3} nitrogen. This spectrum differs from that in Fig. 16 by the appearance of the N-N-pair bound-exciton lines beginning at about 200 °K.

process identification at room temperature depends most strongly on the establishment of the energy balance given by Eq. (4). This balance indicates that the peak position for the bound-exciton process does not shift with temperature. As can be seen in Figs. 14 and 15, the spectral features ascribed to the bound-exciton transitions do not change position with respect to the free-exciton band gap as a function of temperature. The uncertainty here is within a few meV. If there were an important free-to-bound recombination involving the nitrogen center, [50] the magnitude of the shift would be expected to be comparable to that seen in the S free-to-bound recombination in Figs. 6, 12, and 13.

All the spectral features clearly resolved in the 100 °K curves can be identified by comparison with the 4 °K curves published in the literature. [19] The principal line in Fig. 14 is the nitrogen-A-line zero-phonon bound-exciton transition followed to lower energies by a series of phonon sidebands. The small peak at − 19 meV (marked by an arrow) is the sulphur C-line bound exciton and this line is missing in the Zn, N spectra in Fig. 15.

Figure 15 shows the typical appearance of the N-N-pair bound-exciton lines in the spectra as the temperature is lowered. Similar spectra are obtained in n-type samples where the net donor concentrations are approximately 5×10^{15} cm^{-3}. Crystals with the net donor concentration above 10^{17} cm^{-3} show spectral behavior as shown in Fig. 15. Although the bound excitons on pairs of nitrogen are important at lower temperatures, at 300 °K they are thermalized significantly to the point where even at 10^{19}-cm^{-3} N concentrations, they make little contribution to the over-all recombination. This situation might change if significantly more nitrogen were incorporated into the crystals (see Sec. III C). [25]

The full decomposition of the room-temperature spectra remains to be discussed. As described in Sec. III C, above 10^{18}-cm^{-3} nitrogen, the spectra obtained are approximately independent of the nitrogen concentration. As can be seen from Fig. 14, a considerable increase in the high-energy side occurs with increasing temperature. We present evidence that this high-energy component is due to an important free-exciton component.

In the 100 °K curve in Fig. 14, the small feature near 0 meV (marked by an arrow) is thought to be the anti-Stokes TA^X bound-exciton phonon-assisted mode. As the temperature increases, most of the additional strength occurs at too high an energy to be consistent with this continuing to be anti-Stokes emission associated with the bound exciton. Anti-Stokes structure was not resolved above 150 °K and

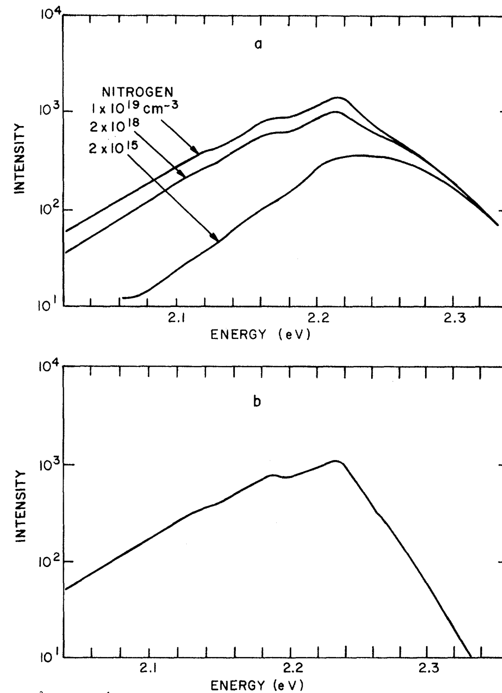

FIG. 16. (a) Comparison of the free-exciton spectra with spectra obtained from crystals with 2×10^{18} and 1×10^{19}-cm^{-3} nitrogen. (b) The nitrogen-bound-exciton spectra resulting from decomposition of free- and bound-exciton processes.

this may result from the overlap of the bound- and free-exciton anti-Stokes processes.

Figure 16(a) shows a comparison of the free-exciton spectra with the spectra as a function of nitrogen concentration. These curves have been normalized together on the high-energy side by matching the line shape. The rather clear evolution of the bound-exciton component out of the free-exciton spectra lends plausibility to the interpretation of the high-energy side resulting from the free-exciton process. By measuring the relative area, one finds the free-exciton component accounts for 40% of the recombination at 2×10^{18}-cm^{-3} nitrogen and 30% at 1×10^{19}-cm^{-3} nitrogen. The slow falloff of the free-exciton component implies that the nitrogen is enhancing the free-exciton recombination rate for nitrogen concentration between 10^{18} and 10^{19} cm^{-3}. This type of impurity-assisted scattering is to be expected. [53] Figure 16(b) shows the spectra due only to the nitrogen-bound-exciton mode obtained by subtracting the free-exciton line shape. The same resultant spectra were obtained for both the 2×10^{18}- and 1×10^{19}-cm^{-3} nitrogen spectra shown in Fig. 16(a).

V. CONCLUSIONS

Spectral measurements of the near-band-gap radiative recombination in GaP on samples configured to eliminate self-absorption effects have been presented. Analysis of the spectra has shown two processes to be important at room temperature. In crystals with nitrogen concentrations lower than 10^{17} cm^{-3}, the dominant emission results from phonon-assisted free-exciton recombination. A weak low-energy feature is contributed by free-to-bound recombination involving shallow neutral donors or acceptors. For nitrogen concentrations greater than 10^{18} cm^{-3}, nitrogen-related recombination processes dominate the emission. The recombination was shown to proceed primarily through a bound-exciton mode but with a free-exciton mode accounting for 30% of the recombination.

ACKNOWLEDGMENTS

We thank R. W. Dixon for helpful discussions during the course of this work and J. V. Rigo for his technical assistance.

[1]R. Z. Bachrach and O. G. Lorimor, J. Appl. Phys. **43**, 500 (1971).

[2]E. E. Loebner and E. W. Poor, Phys. Rev. Lett. **3**, 23 (1959).

[3]H. G. Grimmeiss, A. Rabenau, and H. Koelmans, J. Appl. Phys. **32**, 2123 (1961).

[4]M. Gershenzen and R. M. Mikuyak, J. Appl. Phys. **32**, 1338 (1961).

[5]M. Gershenzen and R. M. Mikulyak, Solid-State Electron. **5**, 313 (1962).

[6]J. W. Allen, M. E. Mancoster, and J. Starkiewicz, Solid-State Electron. **6**, 95 (1963); M. R. Lorenz, T. N. Morgan, M. H. Pilkuhn, and G. D. Pettit, J. Phys. Soc. Jap. Suppl. **21**, 283 (1966).

[7]L. M. Foster and M. Pilkuhn, Appl. Phys. Lett. **7**, 65 (1965).

[8]P. J. Dean, M. Gershenzon, and G. Kaminsky, J. Appl. Phys. **38**, 5332 (1967).

[9]R. C. Taylor, J. F. Woods, and M. R. Lorenz, J. Appl. Phys. **39**, 5404 (1968).

[10]R. A. Logan, H. G. White, and W. Wiegmann, Appl. Phys. Lett. **13**, 139 (1968); Solid-State Electron. **14**, 55 (1971).

[11]K. K. Shih and G. D. Pettit, J. Appl. Phys. **39**, 5025 (1968).

[12]D. R. Wight, J. Phys. C **1**, 1759 (1968).

[13]L. A. Angelova, V. S. Vivilov, Z. Vyberny, and A. E. Yunevick, Sov. Phys.-Semicond. **1**, 877 (1968).

[14]E. G. Dierschke and G. L. Pearson, J. Appl. Phys. **41**, 34 (1970).

[15]M. G. Craford, W. O. Groves, A. H. Herzog, and D. E. Hill, J. Appl. Phys. **42**, 2751 (1971).

[16]C. D. Mosby, E. C. Lightowlers, and G. Davies, J. Lumin. **4**, 29 (1971).

[17]R. Z. Bachrach (unpublished). Kinetic modeling of the green quantum efficiency also substantiates this result.

[18]D. G. Thomas, J. J. Hopfield, and C. J. Frosch, Phys. Rev. Lett. **15**, 857 (1965).

[19]D. G. Thomas and J. J. Hopfield, Phys. Rev. **150**, 680 (1966).

[20]H. C. Casey, Jr., and F. A. Trumbore, Mater. Sci. Eng. **6**, 69 (1970).

[21]O. G. Lorimor, L. R. Dawson, R. Z. Bachrach, D. D. Roccasecca, and R. G. Sobers (unpublished).

[22]R. Z. Bachrach, O. G. Lorimor, L. R. Dawson, and K. K. Wolfstirn, Bull. Am. Phys. Soc. **16**, 436 (1971); J. Appl. Phys. (to be published).

[23]J. D. Cuthbert and D. G. Thomas, Phys. Rev. **154**, 763 (1967).

[24]E. C. Lightowlers, J. Electron. Mater. **1**, 39 (1972).

[25]R. Nicklin, C. D. Mosby, G. Lidgard, and P. B. Hart, in Abstracts of the Solid State Device Conference, U. of Lancaster, 1971 (unpublished). A VPE sample (grown by L. Luther, Bell Telephone Laboratory) examined in this work showed a nitrogen concentration four times higher than has been measured in LPE crystals. This tends to substantiate the general trend found by Nicklin *et al.*

[26]R. Z. Bachrach, Rev. Sci. Instrum. **43**, 734 (1972).

[27]W. B. Joycé, R. Z. Bachrach, and R. W. Dixon, *Optical Extraction Efficiency of Electroluminescent Diodes* (IEDM, Washington, D. C., 1971), paper 10.4.

[28]J. J. Hopfield, D. G. Thomas, and M. Gershenzen, Phys. Rev. Lett. **10**, 162 (1963); and D. G. Thomas, M. Gershenzen, and F. A. Trumbore, Phys. Rev. **133**, A269 (1964).

[29]D. G. Thomas, J. J. Hopfield, and W. M. Augustynlak, Phys. Rev. **140**, 202 (1965).

[30]M. Gershenzen, R. M. Mikulyak, R. A. Logan, and P. W. Foy, Solid-State Electron. **7**, 113 (1964).

[31]K. Colbow, Phys. Rev. **141**, 742 (1966).

[32]P. J. Dean and D. G. Thomas, Phys. Rev. **150**, 690 (1966).

[33]P. J. Dean, G. Kaminsky, and R. B. Zetterstrom, J. Appl. Phys. **38**, 3551 (1967).

[34]M. R. Lorenz, G. D. Pettit, and R. C. Taylor, Phys. Rev. **171**, 876 (1968).

[35]R. S. Knox, *Theory of Excitons* (Academic, New York, 1963).

[36]A. S. Barker, Jr., Phys. Rev. **165**, 917 (1968).

[37]L. Patrick and P. J. Dean, Phys. Rev. **188**, 1254 (1969).

[38]R. Z. Bachrach and J. S. Jayson, Phys. Rev. (to be published).

[39]B. L. Joesten and F. C. Brown, Phys. Rev. **148**, 919 (1966).

[40]P. J. Dean, G. Kaminsky, and R. B. Zetterstrom, Phys. Rev. **181**, 1149 (1969).

[41]R. N. Bhargava, Phys. Rev. B **2**, 387 (1970).

[42]J. Dishman, Phys. Rev. B **3**, 2588 (1971).
[43]J. S. Blakemore, *Semiconductor Statistics* (Pergamon, New York, 1962).
[44]A. Onton, Phys. Rev. **186**, 786 (1969).
[45]P. J. Dean, C. J. Frosch, and C. H. Henry, J. Appl. Phys. **39**, 5631 (1968).
[46]D. G. Thomas, M. Gershenzon, and F. A. Trumbore, Phys. Rev. **133**, A269 (1964).
[47]P. J. Dean, R. A. Faulkner, S. Kimura, and M. Illegams, Phys. Rev. B **4**, 1926 (1971).
[48]J. S. Jayson and R. Z. Bachrach, Phys. Rev. B **4**, 477 (1971).
[49]J. M. Dishman, Phys. Rev. B **5**, 2258 (1972).
[50]M. DiDomenico, J. M. Dishman, and K. P. Sinha, Phys. Rev. B **3**, 1270 (1971).
[51]T. N. Morgan, Phys. Rev. Lett. **21**, 819 (1968).
[52]A. T. Vink, A. J. Bosman, J. A. W. Van der Does de Bye, and R. C. Peters, J. Lumin. **5**, 57 (1972).
[53]R. A. Faulkner, Phys. Rev. **175**, 991 (1968).

PHYSICAL REVIEW B VOLUME 7, NUMBER 2 15 JANUARY 1973

Muonium in Silicon and Germanium—a Deep Donor

J. Shy-Yih Wang and C. Kittel*
Department of Physics, University of California, Berkeley, California 94720
(Received 22 August 1972)

The hyperfine splitting of muonium in Si and Ge is analyzed on various models of the dielectric properties of the medium. Muonium acts as a deep donor in Si and Ge, contrary to some earlier predictions. It is possible to give a reasonable account of the observed values of $|\psi(0)|^2$ in terms of the Reiss–Kaus cavity models, and in terms of the Walter–Cohen $\epsilon(q)$ calculated from the actual band structures, provided that the electron mass is taken as essentially equal to the free-electron mass. Identical results are expected for interstitial atomic hydrogen.

I. INTRODUCTION

Muonium, a hydrogenlike atom composed of an electron and a positive muon, is formed in solids when a muon comes to rest. The hyperfine splitting of muonium can be measured with considerable accuracy by studying the precession of the spin in a magnetic field. This precession is revealed by the direction of the positron emitted in the decay reaction $\mu^+ \rightarrow e^+ + \bar{\nu}_\mu + \nu_e$, with a lifetime of 2.2 μsec. From a Fourier analysis of the precession signal it is possible to obtain the value of the hyperfine splitting of the ground state of the muonium atom in the medium. From the observed hyperfine splitting and the contact hyperfine equation one finds an experimental value for $|\psi(0)|^2$, the probability density of the electron at the muon.

Such experiments were first carried out by Gurevich and co-workers.[1,2] They found, for example, that the hyperfine splitting of muonium in ice (4791 ± 300 MHz) and in fused quartz (4404 ± 70 MHz) are not far from the splitting in vacuum (4463 MHz) and lead to values of $|\psi(0)|^2$, consistent with values observed by EPR for atomic hydrogen in the same media.

The story is different for muonium in germanium and silicon. In germanium Gurevich and co-workers[2] at Dubna found

$$|\psi(0)|^2_{\text{Ge}}/|\psi(0)|^2_{\text{vac}} = 0.58 \pm 0.04 ,$$

and for silicon Crowe and co-workers[3] at Lawrence Berkeley Laboratory found

$$|\psi(0)|^2_{\text{Si}}/|\psi(0)|^2_{\text{vac}} = 0.444 \pm 0.020 .$$

It is seen from these values that the effects of the medium are important in Ge and Si as compared to ice and fused quartz. It is not possible at present to compare these values with those for atomic hydrogen in germanium and in silicon for the simple reason that the presence of atomic hydrogen in these crystals has never actually been detected by a direct physical measurement, to our knowledge.[4] We expect that the donor states will be identical for H as for muonium, so that the hyperfine splittings should be near 630 and 820 MHz, as compared with the vacuum splitting 1420 MHz.

It has been widely believed[5] that hydrogen may be the most common impurity in crystals of Ge and Si normally considered pure. In the un-ionized state the H or H_2 would not affect the electrical properties. It is known that Ge and Si are permeable to hydrogen at elevated temperatures,[6] and there is some hope that it can be quenched in these crystals by rapid cooling. (The criterion for successful quenching is essentially that the phonons should diffuse out of the crystal faster than the hydrogen.) However, at the moment of writing we know more about muonium in Ge and Si than about H or H_2 in just these crystals on which rests most of modern solid-state electronics technology. Unfortunately we do not know the ionization energy of either muonium or H in Ge or Si, so we have to draw our conclusions only from the experimental values of $|\psi(0)|^2$.